

Rate limit of protein elastic response is tether dependent

Ronen Berkovich^{a,1,2}, Rodolfo I. Hermans^{a,b,1}, Ionel Popa^a, Guillaume Stirnemann^c, Sergi Garcia-Manyes^{a,d}, Bruce J. Berne^{c,2}, and Julio M. Fernandez^{a,2}

^aDepartment of Biological Sciences, Columbia University, New York, NY 10027; ^bLondon Centre for Nanotechnology, University College London, London WC1H 0AH, United Kingdom; ^cDepartment of Chemistry, Columbia University, New York, NY 10027; and ^dDepartment of Physics and Randall Division of Cell and Molecular Biophysics, King's College London, London WC2R 2LS, United Kingdom

Contributed by B. J. Berne, July 18, 2012 (sent for review June 21, 2012)

The elastic restoring force of tissues must be able to operate over the very wide range of loading rates experienced by living organisms. It is surprising that even the fastest events involving animal muscle tissues do not surpass a few hundred hertz. We propose that this limit is set in part by the elastic dynamics of tethered proteins extending and relaxing under a changing load. Here we study the elastic dynamics of tethered proteins using a fast force spectrometer with sub-millisecond time resolution, combined with Brownian and Molecular Dynamics simulations. We show that the act of tethering a polypeptide to an object, an inseparable part of protein elasticity *in vivo* and in experimental setups, greatly reduces the attempt frequency with which the protein samples its free energy. Indeed, our data shows that a tethered polypeptide can traverse its free-energy landscape with a surprisingly low effective diffusion coefficient $D_{\text{eff}} \sim 1,200 \text{ nm}^2/\text{s}$. By contrast, our Molecular Dynamics simulations show that diffusion of an isolated protein under force occurs at $D_{\text{eff}} \sim 10^8 \text{ nm}^2/\text{s}$. This discrepancy is attributed to the drag force caused by the tethering object. From the physiological time scales of tissue elasticity, we calculate that tethered elastic proteins equilibrate *in vivo* with $D_{\text{eff}} \sim 10^4\text{--}10^6 \text{ nm}^2/\text{s}$ which is two to four orders magnitude smaller than the values measured for untethered proteins in bulk.

force spectroscopy | protein diffusion | viscoelasticity | single molecule

While the dynamics of proteins have been studied in detail using bulk techniques their behavior when tethered and placed under force is still poorly understood. Tissue elasticity in living organisms results from the extension and recoil of proteins that are tethered to rigid structures that move under force. For example, the giant protein titin responsible for the elasticity of muscle, is mechanically anchored to both the Z disk and the M-line of the half-sarcomere (1), responding to a mechanical perturbation by elastically changing the end-to-end length (2). Hence, it is likely that one of the limiting factors in the physiological activity of a muscle fiber is ultimately determined by the dynamics of the elastic recoil of an extended and tethered polypeptide. Hummingbirds flip their wings by up to 80 Hz, and insects up to 800 Hz (3). It is interesting here to consider that the fastest muscle-driven wing beat rates never surpass a kilohertz (3). Other types of physiological activities also appear to be capped at a similar time scale. For example, salamanders can shoot and fully extend their tongues out in less than 7 ms in order to catch flying prey (4). Throughout these physiological activities it is essential that the extending polypeptide remains elastic. If at any time the speed of the muscle motion exceeded the relaxation time of the polypeptide, the muscle will cease to be elastic, greatly affecting its ability to provide a restoring force, and to store energy. For example, a significant part of the turkey's stride results from energy stored in the passive elasticity of muscle (5). In light of these observations, it is interesting to determine the extent to which these physiological limits can be explained in terms of the diffusional dynamics of the tethered extending polypeptides.

The elasticity of a polypeptide is typically modeled using either the worm-like-chain (WLC) (6, 7) or the freely-jointed-chain models of polymer elasticity (2), where the dynamics of equilibration is assumed to be instantaneous compared to the physiological time scales. This assumption can be justified given that bulk studies of untethered proteins using Förster resonance energy transfer (FRET) probes have conclusively measured the diffusional dynamics of single polypeptides and shown that freely diffusing proteins equilibrate with a very fast diffusion coefficient of $D \sim 10^7\text{--}10^8 \text{ nm}^2/\text{s}$ (8–11). It is therefore not surprising that some theoretical studies modeling the elastic behavior of proteins use the values of D measured from untethered protein in bulk (12, 13).

A recent attempt was made to measure the internal friction of extended proteins tethered to Atomic Force Microscope (AFM) cantilevers (14, 15). Although these experiments had a limited time resolution ($>10 \text{ ms}$), the authors made an effort to subtract the contributions made by the cantilever in order to get an estimate of the protein's internal friction. These experiments estimated an internal friction at 100 pN, predicting values of $D \sim 10^3 \text{ nm}^2/\text{s}$ for the tethered protein, which is five orders of magnitude smaller than those measured by FRET experiments. Other authors have used force spectroscopy techniques to measure the elastic dynamics of tethered polypeptides resulting in values of $D \sim 10^2\text{--}10^4 \text{ nm}^2/\text{s}$ (16–18). As a consequence, some theoretical work of proteins under force used very low values of $D \sim 1,200 \text{ nm}^2/\text{s}$ (19, 20) to match the results obtained from force spectroscopy. Similarly, a value of approximately $10^4 \text{ nm}^2/\text{s}$ was needed to explain the dynamics of riboswitches tethered onto optical tweezers beads (21). Thus, the diffusional dynamics of a protein estimated from bulk techniques and from force spectroscopy techniques are very disparate.

It is surprising that these contradictory results have not been questioned before. In spite of its importance for understanding tissue elasticity, the effect of tethering on the internal dynamics of a protein is still not understood. We probe the elasticity of single extended polypeptides in the submillisecond range using a fast force-spectrometer, which provides a 20-fold improvement in time resolution, in combination with Brownian dynamics and Molecular Dynamics simulations (MD). MD simulations suggest that diffusion of an isolated protein under force occur on a very fast time scale ($D \sim 10^8 \text{ nm}^2/\text{s}$), in agreement with FRET measurements. These simulations were done by applying force to a single atom in the terminal end of the protein and measuring

Author contributions: R.B., R.I.H., I.P., G.S., S.G.-M., B.J.B., and J.M.F. designed research; R.B., R.I.H., I.P., G.S., and S.G.-M. performed research; R.B., R.I.H., I.P., G.S., and S.G.-M. analyzed data; and R.B., R.I.H., I.P., G.S., S.G.-M., B.J.B., and J.M.F. wrote the paper.

The authors declare no conflict of interest.

¹R.B. and R.I.H. contributed equally to this work.

²To whom correspondence may be addressed. E-mail: rb2825@columbia.edu or bb8@columbia.edu or jfernandez@columbia.edu.

This article contains supporting information online at www.pnas.org/lookup/suppl/doi:10.1073/pnas.1212167109/-DCSupplemental.

the resulting changes in length (22). However, freely diffusing polypeptides measured in bulk are far from representing the physics of elastic proteins such as titin, which by definition must always be tethered to larger structures that move in conjunction. Here we demonstrate that the large slowing down of the diffusional dynamics of a protein as measured in AFM experiments is due to the drag force exerted by the object to which it is tethered. We therefore suggest that the slow dynamics probed in force spectroscopy is an inherent property of tethering a protein to a solid object, of widespread significance for understanding the dynamics of tissue elasticity.

Results and Discussion

The advent of force-clamp spectroscopy has made it possible to probe the dynamics of single proteins extending and relaxing under a well defined force (23). This approach now permits a direct study of the relaxation times of a polypeptide under a rapid load change. However, the published response times of the feedback in force spectrometers ranges from 5–10 ms for fast AFMs (23) and up to approximately 100 ms for optical tweezers instruments (24). Although the current instrumentation can comfortably measure the kinetics of protein unfolding and refolding, it is far too slow to probe the recoil dynamics of a stretched polypeptide under force. The main limitations have been the frequency response of the piezoelectric actuators and of the cantilevers used in the AFM instruments. Here we built a new force-clamp apparatus (Fig. 1A) that makes use of a fast piezoelectric actuator (>300 kHz) and small Olympus cantilevers with resonant frequencies >10 kHz. The set-up can settle the applied force within approximately 150 μ s (see *SI Text*).

Our experimental design consists of first unfolding and extending a single ubiquitin polypeptide at a force of 180 pN, resulting in a series of step increases in length of approximately 20 nm (23). This staircase uniquely identifies the ubiquitin protein and also verifies that force is applied to a single polypeptide chain (Fig. 1B). Once a poly-ubiquitin protein is fully extended, the polypeptide was repeatedly cycled between 250 pN and 100 pN in order to measure the relaxation and extension dynamics (Fig. 1B). At these high forces, the polypeptide always remains highly extended. We averaged and merged all the repeating cycles of recoil and reextension such that we obtained a smoothed recoil (blue) and extension (green) trace (Fig. 1C; top traces). A similar procedure was used to average and merge the force steps over the same trace (Fig. 1C; bottom traces). The response time achieved by the new force clamp instrumentation is shown in Fig. 1C, where approximately 70% of the command force settles with a time constant of approximately 20 μ s. The residual creep in the force settles more slowly with a time constant of 1.1 ms. The observed oscillations are due to the main resonant mode of the system, as the instrument approaches the limit of its operating bandwidth (approximately 7 kHz). Crucially, the polypeptide relaxes more slowly than the force with an exponential time course with a time constant of $\tau = 1.17$ ms. The polypeptide reextends with a faster time course ($\tau = 0.68$ ms), while the averaged force traces appear identical. Our protocol cycles an extended polypeptide between two well defined regions of the potential of mean force (PMF), calculated from the WLC model of polymer elasticity and the applied force (25, 26) (Fig. 1D; 1–4). The PMF slope is steeper at the higher force of 250 pN (4 to 1 in Fig. 1D), which causes a faster rate of extension when compared to the rate of recoil at 100 pN (2 to 3 in Fig. 1D). This asymmetry suggests that our recordings are reporting on the underlying PMF of the polypeptide, in the millisecond time scale, as also illustrated by our MD simulations (see below).

In Fig. 2A we fit single exponentials to recoil trajectories measured at 100 pN and extension trajectories measured at 250 pN. The polypeptides can be of very different contour lengths, L_c , due to the varying length of the polypeptides that are picked up

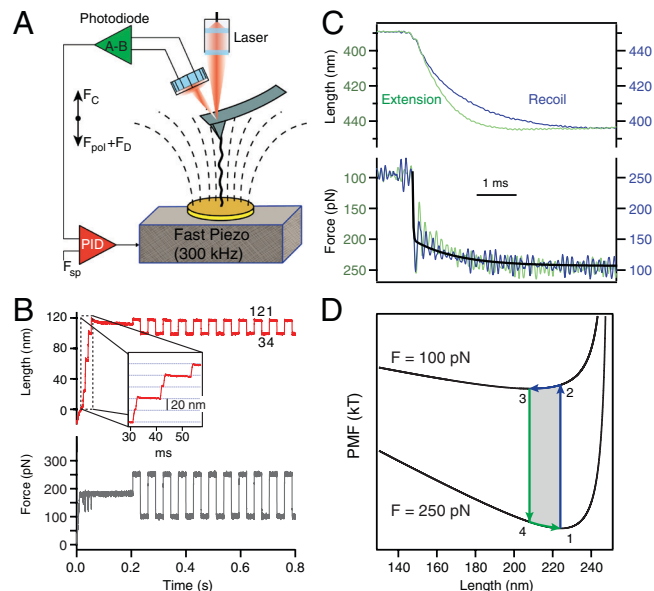


Fig. 1. Experimental design for time resolved measurements of the recoil dynamics of an extended polypeptide. (A) Schematic diagram of the force-clamp apparatus. A single polypeptide is extended between a high-speed cantilever (Olympus biolever) and a piezoelectric actuator with a high resonant frequency (300 kHz, Physik Instrumente PL-055.30). A well-tuned PID amplifier adjusts the piezoelectric actuator so as to keep the force on the polypeptide at the set point value (F_{sp}). Under force clamp conditions, $F_c = F_{pol} + F_D$, where F_c is the force applied by the cantilever, F_{pol} is the elastic force produced by the molecule and F_D is the flow drag force (dashed lines) from the motion of the piezoelectric actuator. (B) Typical experimental trace of the end-to-end length corresponding to the force protocol on the lower box. The inset shows a staircase of ubiquitin unfolding events (stars) measured at 180 pN providing a strong fingerprint for a single polypeptide and measures its initial length. The extended polypeptide is then repeatedly cycled between 250 pN and 100 pN in order to collect many trajectories ($7 < n < 30$) until the molecule detaches. (C) Example of a recoil trajectory (blue) obtained by averaging eight consecutive recoil trajectories. The averaged force trace shows a step (250 pN down to 100 pN) with a half time of approximately 33 μ s, which is more than 10 times shorter than the relaxation time constant of the polypeptide measured to be approximately 1.11 ms. After recoil, the corresponding extension (green trace) is much faster with a time constant of approximately 0.68 ms. The force traces are superimposable. (D) Potential of mean force of a 250 nm long polymer calculated at two pulling forces of 250 pN and 100 pN, using the WLC model of polymer elasticity (lower box). The figure highlights the physics of our experimental design. The polypeptide starts extended at 250 pN (1) and then it is abruptly relaxed to 100 pN (2) where it recoils down to its new minimum (3), then it is switched back to the high force (4) where it extends to the PMF minimum at 250 pN (1).

by the AFM cantilever. Thus, we can measure the relaxation time constant, τ , as a function of the contour length of the polypeptide for both types of trajectories (Fig. 2B). The results show that the value of τ grows linearly with L_c , for both the recoil and extension trajectories, albeit with very different slopes (filled circles and triangles respectively; Fig. 2B). The linear dependency of τ vs. L_c can be explained by the scaling of the PMF with the contour length of the polypeptide, where the distance between minima at 250 pN and 100 pN (ΔL ; inset of Fig. 2B), increases linearly with the contour length. These measurements clearly indicate that the extended polypeptide equilibrates at each new force by sampling its PMF.

Here we examine whether simple Brownian dynamics based on the PMF predicted by the WLC model can account for the time scales of relaxation of the extended polypeptides as they adjust to a new force. The time course of the end-to-end length of a model polypeptide is calculated by solving the stochastic equation of motion:

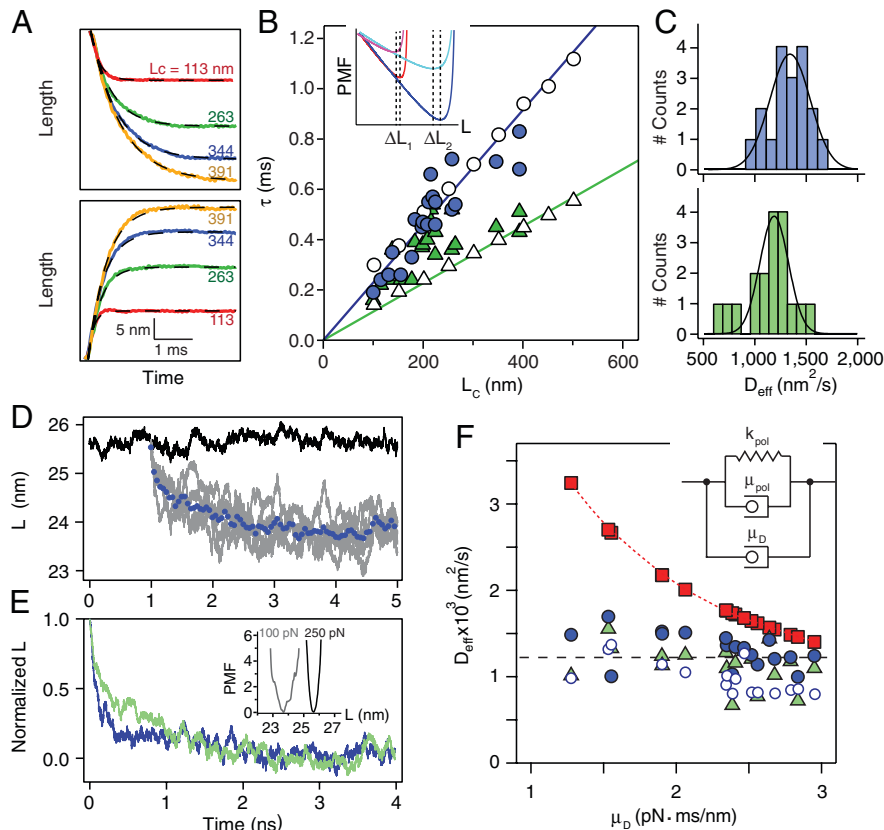


Fig. 2. Time constants and diffusion coefficients from extension and recoil traces of single polypeptides. (A) A series of four different recoil (upper box) and extension (lower box) trajectories measured from extended polypeptides of different contour lengths L_c (as labeled; 113 nm, 263 nm, 344 nm, and 391 nm). The data were fit with a single exponential to measure the value of the relaxation time constant, τ , (dashed lines). (B) Relaxation (filled circles) and extension (filled triangles) time constants, τ , as a function of the contour length of the polypeptide L_c . The asymmetry of the potential shown in Fig. 1D, results into very different values of τ for the extension and recoil, as shown in Fig. 1B. The linear contour length dependency of τ is readily reproduced by Brownian dynamics simulations using the potential shown in Fig. 1D and the values of D_{eff} measured from these data (open circles and triangles). The linear dependency of D_{eff} on L_c results from that of the total travel (ΔL) on L_c (inset). (C) Histograms of values for D_{eff} measured from the recoil (top box) and extension (bottom box) traces shown in Fig. 2A. (D and E) MD simulations of the end-to-end length as a function of time for ubiquitin maintained at a constant force of 250 pN (D; black curve); relaxation after force is quenched from 250 pN to 100 pN (D; grey curves) and averaged over five such trajectories (D; blue dots). Even if each of the time-origins of each trajectory differs, we make them coincide in the plot for clarity. (E) Normalized recoil (green curve) and extension (blue curve) averaged over five trajectories. The inset shows the PMF along the end-to-end distance at 100 pN (gray curve) and 250 pN (black curve). Both curves are shifted so that their minimum is 0. (F) Plot of the measured values of D_{eff} (circles from recoils; triangles from extensions) as a function of the viscoelastic drag, μ_D , measured from each cantilever. The upper squares show the values of $D_{\text{max}} = k_B T / \mu_D$, marking the upper limit of D measured for each cantilever. We attribute the difference between D_{eff} and D_{max} to the noninstantaneous force step of the force-clamp apparatus. The open circles show the values of D_{eff} measured from BD simulations that include the time course of the force-step for each experiment. The inset portrays a simplified mechanical representation of the principal contributions to the forces of an extending polypeptide during these experiments. The Voigt model representing the polypeptide (k_{pol} , μ_{pol}) is in parallel with the drag (μ_D) generated by the motion of the piezoelectric actuator, giving $\mu_{\text{eff}} = \mu_{\text{pol}} + \mu_D$.

$$\frac{dx}{dt} = -\frac{D_{\text{eff}}}{p} \left[\frac{1}{4} \left(1 - \frac{x}{L_c} \right)^{-2} - \frac{1}{4} + \frac{x}{L_c} \right] + \frac{D_{\text{eff}} F_i}{k_B T} + \Gamma(t), \quad [1]$$

where $x(t)$ is the one-dimensional end-to-end reaction coordinate, D_{eff} is the effective diffusion coefficient, p is the persistence length set to 0.4 nm, F_i is the applied force, k_B is Boltzmann's constant, T is the absolute temperature, and $\Gamma(t)$ is white noise with $\langle \Gamma(t) \rangle = 0$ and correlation time $\langle \Gamma(t) \Gamma(t') \rangle = 2D_{\text{eff}} \delta(t - t')$. We completed a set of simulations where the force was switched between 250 pN and 100 pN and the contour length L_c was varied from 100 nm to 500 nm. We fitted single exponentials to the simulated extensions and relaxations and measured the resulting time constants (open triangles and circles respectively; Fig. 2B). Simulations using a fixed value of $D_{\text{eff}} = 1,226 \text{ nm}^2/\text{s}$ (see below), matched the observed trends in our data, readily reproducing the difference in time constants between relaxation and extension and their linear growth with contour length (Fig. 2B). We also estimated the value of D_{eff} directly from each relaxation trace with a simple high force approximated solution to Eq. 1 as

$$x(t) = x_f - AW \left\{ -B \exp \left[-\frac{D_{\text{eff}}}{2pL_c} \left(\frac{4pF_i}{k_B T} \right)^{3/2} (t - t_0) \right] \right\}, \quad [2]$$

where W is the Lambert W function which is defined to be the multivalued inverse of the function $z = W(z)e^{W(z)}$ (27), x_f is the final protein length after the relaxation, A and B are fitting parameters, and t_0 is the time at which the force was changed. Fits of Eq. 2 to the relaxation data shown in Fig. 2A gave a distribution of D_{eff} values for both types of relaxation (Fig. 2C). The fitted values indicate a mean of $1,317 \pm 197 \text{ nm}^2/\text{s}$ for the recoil and $1,135 \pm 234 \text{ nm}^2/\text{s}$ for the extension traces, giving an average value of approximately $1,226 \text{ nm}^2/\text{s}$, which was used in the simulations of Fig. 2B. Our observations support the view that a tethered polypeptide samples its PMF with a diffusion coefficient of $D_{\text{eff}} \sim 10^3 \text{ nm}^2/\text{s}$, which is in surprisingly close agreement with previous measurements using tethered proteins (14–18).

The measured values of D_{eff} for tethered polypeptides are 4–5 orders of magnitude smaller than those measured from studies of polypeptides in bulk using FRET techniques (8–11). Indeed,

if we use a value of $D_{\text{eff}} \sim 10^8 \text{ nm}^2/\text{s}$ in our Brownian dynamics simulations, the resulting relaxation times are in the nanosecond time scale, far from those observed experimentally. Nevertheless, it could be argued that diffusion of an extended protein under force is a much slower process than the diffusion of unfolded proteins in solution as studied by FRET. To gain more insight into these discrepancies, we did all-atom MD simulations in explicit solvent of ubiquitin relaxation under force (see *SI Text* for details). When kept under a constant force of 250 pN, the protein is fully extended and its end-to-end distance fluctuates around an average value of $L = 25.5 \text{ nm}$ (Fig. 2D, black trace). At given moment along this trajectory, we quenched the force to a lower value of 100 pN while monitoring the relaxation of L (Fig. 2D, gray traces). These trajectories, starting from different initial configurations, were averaged to recover an average profile (Fig. 2D, blue points). It is clear that L relaxes on a nanosecond time scale, in stark contrast with the millisecond relaxation observed by our experiments, before it fluctuates around a new average value of $L = 23.7 \text{ nm}$ at 100 pN. Importantly, we checked that L does not further decay during a much longer simulation of 30 ns. Fitting these two lengths with the WLC predictions gives a contour length $L_c = 28.4 \text{ nm}$ and a persistence length $p = 0.38 \text{ nm}$, in agreement with values usually measured experimentally (28, 29), suggesting that the full relaxation of the end-to-end distance was being reached.

We then explored the reverse scenario where the protein equilibrated at 100 pN is pulled at a constant force of 250 pN. The renormalized average of several such traces allowed direct comparison with the normalized recoil profile (Fig. 2E). The slower relaxation compared to the extension shows that AFM experiments and MD simulations are probing the same PMF. For both forces, the PMF extracted from the end-to-end distributions of equilibrium simulations further proves this point. The PMF at 250 pN is significantly stiffer than that at 100 pN, in agreement with the WLC predictions (Fig. 1D) and explains why the extension (i.e., motion along the 250 pN free energy surface) is faster than relaxation (motion along the 100 pN free-energy surface).

Independently from these extension/relaxation simulations, we estimated the diffusion coefficient along the end-to-end distance close to the minimum of each free-energy basin (see *SI Text* for details). The obtained values are $D_{\text{pol}} = (5.3 \pm 1.4) \cdot 10^8 \text{ nm}^2/\text{s}$ for $L = 23.7 \text{ nm}$ and $F = 100 \text{ pN}$, and $D_{\text{pol}} = (4.2 \pm 1.1) \cdot 10^8 \text{ nm}^2/\text{s}$ for $L = 25.5 \text{ nm}$ and $F = 250 \text{ pN}$. The obtained values are in close agreement with those measured in FRET experiments, but 5 to 6 orders of magnitude larger than those measured in our AFM experiments. Even if our method to estimate D_{pol} may suffer from uncertainties and other force fields may lead to some differences in the measured time scale, these factors cannot in any case explain the 6 order of magnitude difference with our experiments.

In order to understand these important discrepancies we must first consider the various contributions to the value of D_{eff} in a protein placed under force. In the simulations, the force is directly applied to one extremity of the protein while the other is being fixed. From an experimental point of view, application of a mechanical force to a polypeptide always must involve the tethering of the polypeptide to a macroscopic object. Motion of the polypeptide is thus intimately tied to motion of the object. Any attempt of the polypeptide to move along the end-to-end length reaction coordinate of the PMF must also displace the object to which the protein is tethered. In our case, the polypeptide is tethered to an AFM cantilever and to a large gold covered surface. Thus, any change in the end-to-end length of the polypeptide must also result in drag generated between the moving surfaces (Fig. 1A). A simplified representation of these combined elements is shown in the inset of Fig. 2F, where the extended polypeptide is represented as a Voigt model with an elastic constant k_{pol} and an internal friction of μ_{pol} . The polypeptide is placed in parallel with

the drag caused by the motion of the tethered objects μ_D , so that friction forces are simply additive. We measured the drag force on a cantilever without attached proteins by simply touching the surface and then rapidly moving it away from the cantilever. These measurements gave a drag of $2.3 \text{ pN}\cdot\text{ms}/\text{nm}$. We also measured the drag in each individual experiment after the protein detached from the cantilever and the surface started to rapidly move away (see *SI Text*). From these measurements we obtained an average value of $2.3 \pm 0.5 \text{ pN}\cdot\text{ms}/\text{nm}$. We plot the measured values of D_{eff} as a function of μ_D for the individual experiments and observe that D_{eff} has a weak dependence on the drag forces (Fig. 2F). If drag forces were the sole limiting factor affecting the motion of the polypeptide, we would expect the values of D_{eff} to rise rapidly as drag is reduced, varying as $1/\mu_D$, which is not the case here. However, as it is apparent in Fig. 1C even in the best cases the force step applied to the polypeptide is far from approaching an ideal Heaviside step. Brownian dynamics simulations using the actual measured raw force traces readily reproduce our data. Fitting Eq. 2 to the resulting relaxation traces recovers the values of D_{eff} measured experimentally (open circles; Fig. 2F).

Thus, it is possible to conclude that despite the considerable improvements in the time resolution of our instrumentation the surprisingly low values of D_{eff} measured using force spectroscopy are still dominated by the drag resulting from the motion of the objects to which the polypeptide is tethered. While in our case these objects are the AFM cantilever and a gold-coated glass coverslide, such drag is an obligatory result of the elasticity of tethered polypeptides, a configuration that is widespread in biology. It is difficult to know the magnitude of the drag forces acting on the individual proteins of intact elastic tissues. However, if we consider the biological bandwidth of 800 Hz as the limit of protein elasticity, we can make some educated guesses of the biological drag coefficients and compare them with those measured in this work.

In order to estimate the drag in biological tissues, we examine the limits to the bandwidth of elastic tissues using a simple model as shown in Fig. 3. We use Brownian dynamics (with $D = 1,300 \text{ nm}^2/\text{s}$) to measure the effect of a small sinusoidal force (10 pN, peak to peak) on the extension dynamics of a prototypical

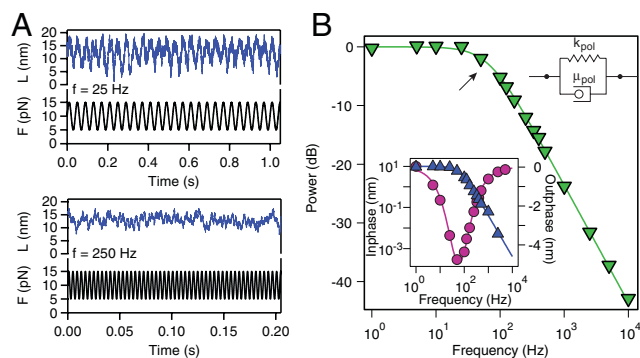


Fig. 3. Bandwidth of an extended polypeptide. (A) Brownian dynamics computes the length of a 30 nm long polypeptide placed under a 10 pN sinusoidal load of varying frequency, f , using the measured value of $D_{\text{pol}} = 1,300 \text{ nm}^2/\text{s}$. The figure shows polypeptide responses at two different frequencies (25 Hz, and 250 Hz). (B) We use lock-in detection to measure the in-phase (ϕ_0 , triangles) and the out-of phase (ϕ_{90} , circles) components of the elastic response of the polypeptide as a function of the load frequency, f . The solid lines (inset), correspond to the real (triangles) and imaginary (circles) parts of the mechanical impedance of a Kelvin-Voigt model (inset), fitted to the data. From ϕ_0 and ϕ_{90} we calculate power as a function of frequency for the polypeptide (triangles). The solid line fits the Kelvin-Voigt model to the data returning values of $D_{\text{pol}} = 1,313 \text{ nm}^2/\text{s}$ and $k_{\text{pol}} = 1.31 \text{ pN}/\text{nm}$. The arrow shows the -3 dB point, giving a bandwidth of 66 Hz. These measurements show that the elasticity of a polypeptide-based material is band-limited to a few hundred Hertz, in good agreement with broadly observed animal behavior.

tethered protein ($L_c = 30$ nm), as a function of the perturbation frequency, f (Fig. 3A). We analyze these traces using standard lock-in detection to measure the output signal components; the in-phase $\phi_0 = \langle L(t) \cdot \sin(2\pi ft) \rangle$ and the out-of-phase $\phi_{90} = \langle L(t) \cdot \cos(2\pi ft) \rangle$ amplitudes of the elastic response (triangles and circles in the lower left inset of Fig. 3B). Fitting with the corresponding real and imaginary parts of the mechanical impedance of a Kelvin-Voigt model (solid lines), $\phi_0 = \text{Re}(f) = Fk_{\text{pol}} / (k_{\text{pol}}^2 + (2\pi f k_B T / D_{\text{pol}})^2)$ and $\phi_{90} = \text{Im}(f) = F(2\pi f k_B T / D_{\text{pol}}) / (k_{\text{pol}}^2 + (2\pi f k_B T / D_{\text{pol}})^2)$ results in a perfect fit. The output power of the polypeptide oscillations calculated in dB as $10 \cdot \log(\text{Amp}^2(f) / \text{Amp}^2(0))$ is shown in Fig. 3B (triangles), where $\text{Amp}^2(f) = \phi_0^2(f) + \phi_{90}^2(f)$. Fitting the data with $10 \cdot \log(1 / (1 + (2\pi f k_B T / k_{\text{pol}} D_{\text{pol}})^2))$ returned values of $D_{\text{pol}} = 1,313$ nm²/s and $k_{\text{pol}} = 1.31$ pN/nm (solid lines; Fig. 3B). Khatri, et al introduced an elegant expression for a frictional WLC elasticity constant $k_{\text{wlc}} = 4/L_c \cdot (p/k_B T)^{1/2} \cdot F^{3/2}$ (15). Substituting for the values of L_c , F , and p used in our simulations we calculate $k_{\text{pol}} = 1.31$ pN/nm in good agreement with our Voigt model fits. However, a Voigt model serves only as a first approximation given that real polypeptides possess multiple relaxation times.

From these considerations we can now establish the concept of elastic bandwidth. As shown in Fig. 3B, the power output follows the typical Lorentzian function of a low-pass filter. We define the corner frequency of the elastic response as being the frequency at which the power decreased by -3 dB, with respect to the power measured at zero frequency. For the simulations shown in Fig. 3A, the elastic bandwidth is 66 Hz. The half power frequency can also be straightforwardly calculated from the above considerations as;

$$f_{1/2} \cong \frac{2D\sqrt{p}}{\pi L_c} \left(\frac{F}{k_B T} \right)^{3/2}, \quad [3]$$

where the elastic bandwidth of a polypeptide grows linearly with D . It is interesting to consider the consequences of Eq. 3. For example, simplifying the complex muscle titin protein to a polypeptide with $L_c = 300$ nm, $p = 0.6$ nm and at $F = 4$ pN (2) and assuming $f_{1/2} \sim 50$ Hz (hummingbird) (3), we calculate a value of $D_{\text{eff}} \sim 10^4$ nm²/s. For the same titin protein operating at the limits of insect motion at $f_{1/2} \sim 800$ Hz would give values of $D_{\text{eff}} \sim 10^6$ nm²/s. Our estimate of the speed limit of a tethered protein in vivo is much larger than that measured in our experimental system but still at least two orders of magnitude smaller than the values obtained by FRET and MD simulations. It is clear that the diffusional constants measured for polypeptides in solution do not apply to tethered polypeptides, and that extended polypeptides sample their PMF with values of D_{eff} that are unique to each system and cannot be generalized.

Fig. 4 summarizes the consequences of tethering a polypeptide to an object in order to establish an elastic system. As described before, the basic PMF for a polypeptide contains an attractive potential that acts mostly at short extensions combined with the potential of the WLC which rapidly becomes dominant as the polypeptide extends (25, 26). At zero force, the PMF is downhill towards the collapsed state. Application of a constant force perturbation modifies the PMF creating an entropic barrier at relatively high extensions that can trap the collapsing polypeptide for some time, before it proceeds downhill towards the fully collapsed state (25, 26, 30). The dynamics of extended polypeptides responding to a change in the force will be determined, to a large extent, by the value of D_{eff} . Molecules tethered to AFM cantilevers such as those used in our work will move along their PMF with values of $D_{\text{eff}} \sim 10^3$ nm²/s (1; Fig. 4), which readily explain our earlier observations (30, 31). It is interesting to consider that

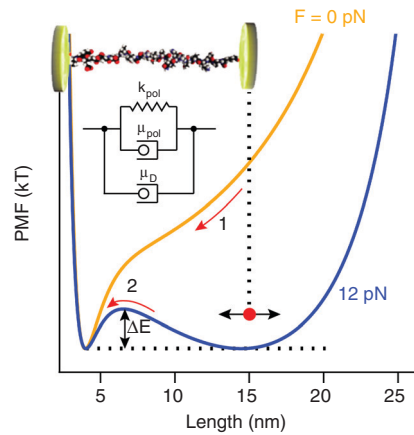


Fig. 4. Effect of tethering on the dynamics of an extending polypeptide. The act of tethering a polypeptide to an object (top inset) is an essential step in constructing an elastic system and introduces drag (μ_D ; bottom inset) in parallel with the molecule (k_{pol} , μ_{pol}). Polypeptide PMF's calculated at $F = 0$ and $F = 12$ pN (25). Any motion of the polypeptide along its PMF will cause drag from the tethered objects, greatly affecting its kinetics both for simple diffusion (1) or for barrier crossing events that significantly change the end-to-end length of the molecule (2).

the value of D_{eff} also affects barrier-crossing events. Indeed, transition state theory predicts that the attempt frequency for barrier-crossing events is given by $D_{\text{eff}}\omega_0\omega_B/2\pi$, where ω_0 and ω_B represent the curvatures of the PMF before the barrier and at the transition state (32). Thus, the kinetics of barrier crossing events that change the end-to-end length [e.g., (2); Fig. 4] will be greatly affected by tethering. An example of such barrier is the entropic barrier created by the force, which crosses over long distances along the PMF (Fig. 4) (30). In this case, the kinetics of barrier crossing will be greatly affected by drag and by the resulting D_{eff} . By contrast, barrier crossing events that do not significantly change the end-to-end length of the molecule will be unaffected by the drag of the tethered objects. Indeed, the mechanical unfolding of ubiquitin which only has to extend by approximately 0.25 nm to cross the unfolding barrier (23) shows a very high attempt frequency (33).

Our observations of the effects of tethering on the value of D_{eff} apply to extended polypeptides where the internal friction of the molecule does not seem to play a significant role. However, under conditions where the internal friction of a polypeptide may become dominant, for example in collapsed molten globule states (34), the effects of tethering should be minimal. Furthermore, although the dynamics of a polypeptide takes place in more than one dimension, the effects of tether-drag will be mostly along the pulling coordinate. Other instruments such as optical tweezers and magnetic tweezers, which tether polypeptides to beads, will also show a substantial amount of drag giving different values of D_{eff} for different bead sizes. Extended polypeptides probed by different instruments will show different dynamics depending of the values of D_{eff} that result from tethering the polypeptide in each unique configuration. Thus, it is important that the drag is characterized in each instrumental configuration, and that its effects are understood and taken into account when analyzing force-spectroscopy data of extended molecules. Most importantly, the dynamics of a molecule whose kinetics is dominated by the drag of the objects to which it is tethered cannot be extrapolated to that of an untethered freely diffusing molecule in bulk. This conclusion is of wide significance for the understanding of the dynamics of numerous proteins that are tethered and under force in vivo.

Materials and Methods

Details about protein engineering and purification, experimental setup, and Brownian dynamics and MD simulations are provided in the [SI Text](#).

ACKNOWLEDGMENTS. We thank Gerard Borst, for sharing his Igor application for the Lambert W function. I.P. acknowledges the Swiss National Science Foundation for a postdoctoral research grant. S.G-M. thanks the Fundación Caja Madrid and IberCaja for financial support. This work was supported by

the National Institutes of Health (NIH) (NIH-HL66030 and NIH-HL61228 to J.M.F.; NIH-GM4330 to B.J.B.) and in part by National Science Foundation (NSF) through TeraGrid resources provided by National Center for Supercomputing Applications and ABE (MCA08X002 to B.J.B.).

- Linke WA (2008) Sense and stretchability: The role of titin and titin-associated proteins in myocardial stress-sensing and mechanical dysfunction. *Cardiovasc Res* 77:637–648.
- Li HB, et al. (2002) Reverse engineering of the giant muscle protein titin. *Nature* 418:998–1002.
- Greenewalt CH (1960) The wings of insects and birds as mechanical oscillators. *Proc Am Philos Soc* 104:605–611.
- Deban SM, Richardson JC (2011) Cold-blooded snipers: Thermal independence of ballistic tongue projection in the salamander hydromantes platycephalus. *J Exp Zool A* 315A:618–630.
- Roberts TJ, Marsh RL, Weyand PG, Taylor CR (1997) Muscular force in running turkeys: The economy of minimizing work. *Science* 275:1113–1115.
- Bustamante C, Marko JF, Siggia ED, Smith S (1994) Entropic elasticity of Lambda-Phage DNA. *Science* 265:1599–1600.
- Rief M, Gautel M, Oesterhelt F, Fernandez JM, Gaub HE (1997) Reversible unfolding of individual titin immunoglobulin domains by AFM. *Science* 276:1109–1112.
- Haas E, Katchalskikatzir E, Steinberg IZ (1978) Brownian-motion of ends of oligopeptide chains in solution as estimated by energy-transfer between chain ends. *Biopolymers* 17:11–31.
- Hagen SJ, Hofrichter J, Szabo A, Eaton WA (1996) Diffusion-limited contact formation in unfolded cytochrome c: Estimating the maximum rate of protein folding. *Proc Natl Acad Sci USA* 93:11615–11617.
- Lapidus LJ, Steinbach PJ, Eaton WA, Szabo A, Hofrichter J (2002) Effects of chain stiffness on the dynamics of loop formation in polypeptides. Appendix: Testing a 1-dimensional diffusion model for peptide dynamics. *J Phys Chem B* 106:11628–11640.
- Moglich A, Joder K, Kiefhaber T (2006) End-to-end distance distributions and intrachain diffusion constants in unfolded polypeptide chains indicate intramolecular hydrogen bond formation. *Proc Natl Acad Sci USA* 103:12394–12399.
- Hummer G, Szabo A (2001) Free energy reconstruction from nonequilibrium single-molecule pulling experiments. *Proc Natl Acad Sci USA* 98:3658–3661.
- Dudko OK, Graham TGW, Best RB (2011) Locating the barrier for folding of single molecules under an external force. *Phys Rev Lett* 107:208301.
- Kawakami M, Byrne K, Brockwell DJ, Radford SE, Smith DA (2006) Viscoelastic study of the mechanical unfolding of a protein by AFM. *Biophys J* 91:L16–L18.
- Khatris BS, et al. (2008) Internal friction of single polypeptide chains at high stretch. *Faraday Discuss* 139:35–51.
- Calderon CR, Harris NC, Kiang CH, Cox DD (2009) Analyzing single-molecule manipulation experiments. *J Mol Recognit* 22:356–362.
- Calderon CP, Harris NC, Kiang CH, Cox DD (2009) Quantifying multiscale noise sources in single-molecule time series. *J Phys Chem B* 113:138–148.
- Guo SL, Li N, Lad N, Desai S, Akhremitchev BB (2010) Distributions of parameters and features of multiple bond ruptures in force spectroscopy by atomic force microscopy. *J Phys Chem C* 114:8755–8765.
- Minh DDL (2006) Free-energy reconstruction from experiments performed under different biasing programs. *Phys Rev E* 74:061120.
- Minh DDL (2007) Multidimensional potentials of mean force from biased experiments along a single coordinate. *J Phys Chem B* 111:4137–4140.
- Lin JC, Thirumalai D (2008) Relative stability of helices determines the folding landscape of adenine riboswitch aptamers. *J Am Chem Soc* 130:14080–14081.
- Sotomayor M, Schulten K (2007) Single-molecule experiments in vitro and in silico. *Science* 316:1144–1148.
- Schlierf M, Li HB, Fernandez JM (2004) The unfolding kinetics of ubiquitin captured with single-molecule force-clamp techniques. *Proc Natl Acad Sci USA* 101:7299–7304.
- Li PTX, Collin D, Smith SB, Bustamante C, Tinoco I (2006) Probing the mechanical folding kinetics of TAR RNA by hopping, force-jump, and force-ramp methods. *Biophys J* 90:250–260.
- Berkovich R, Garcia-Manyes S, Urbakh M, Klafter J, Fernandez JM (2010) Collapse dynamics of single proteins extended by force. *Biophys J* 98:2692–2701.
- Hyeon CB, Morrison G, Pincus DL, Thirumalai D (2009) Refolding dynamics of stretched biopolymers upon force quench. *Proc Natl Acad Sci USA* 106:20288–20293.
- Corless RM, Gonnet GH, Hare DEG, Jeffrey DJ, Knuth DE (1996) On the Lambert W function. *Adv Comput Math* 5:329–359.
- Li HB, et al. (2001) Multiple conformations of PEVK proteins detected by single-molecule techniques. *Proc Natl Acad Sci USA* 98:10682–10686.
- Walther KA, et al. (2007) Signatures of hydrophobic collapse in extended proteins captured with force spectroscopy. *Proc Natl Acad Sci USA* 104:7916–7921.
- Berkovich R, Garcia-Manyes S, Klafter J, Urbakh M, Fernandez JM (2010) Hopping around an entropic barrier created by force. *Biochem Biophys Res Commun* 403:133–137.
- Fernandez JM, Li HB (2004) Force-clamp spectroscopy monitors the folding trajectory of a single protein. *Science* 303:1674–1678.
- Kramers HA (1940) Brownian motion in a field of force and the diffusion model of chemical reactions. *Physica* 7:284–304.
- Popa I, Fernandez JM, Garcia-Manyes S (2011) Direct quantification of the attempt frequency determining the mechanical unfolding of ubiquitin protein. *J Biol Chem* 286:31072–31079.
- Ptitsyn OB (1995) Molten globule and protein folding. *Adv Protein Chem* 47:83–229.

Supporting Information

Berkovich et al. 10.1073/pnas.1212167109

SI Text

Protein Engineering and Purification. The polyubiquitin Ubi₁₂ construct was engineered as previously described (1). The protein was expressed in BLR *Escherichia coli* cells (Novagen). The cells were grown to OD⁶⁰⁰ of 0.6 at 37 °C and the protein expression was induced with 1 mM isopropyl-1-thio-β-D-galactopyranoside (IPTG) for 3 h at 37 °C. The protein was purified using a Cobalt affinity Talon resin (GE Biosciences) and Fast Fluid Liquid Chromatography (FPLC–Superdex 200 HR column). We used standard phosphate buffered saline for both purification and measurements. All the reagents used had a molecular biology grading.

Experimental Setup. The measurements were obtained using an atomic force microscope (AFM) customized for high-speed single molecule force spectroscopy. The present AFM configuration distinguishes itself from commonly used AFM spectrometers through the use of smaller cantilevers, faster piezoelectric actuators, a horizontal configuration, and a double-pulse preemptive control system customized for the intended experimental protocol. In order to decouple the force measurements from the main oscillatory mode of the supporting optical table the sample substrate was mounted vertically i.e., the substrate normal and the force measurements were all in a direction parallel to the optical table's surface and therefore perpendicular to the observed dominant perturbations in the vertical axis.

The substrate was attached to a specially designed stage composed of two piezoelectric actuators mounted in series. A slow piezoelectric actuator (PicoCube, Physik Instrumente) with a travel of 6 μm was used for cantilever calibration, to approach the surface to the cantilever and for lateral movement. A second piezoelectric actuator mounted between the first one and the surface (PL055.30 multi-layer piezo stack, Physik Instrumente) with a travel of 2 μm and a nominal resonant frequency higher than 300 kHz was used to obtain the constant force condition with a high response time. In the force clamp mode the force is controlled by a feedback loop. The measured force signal is fed into a well-tuned analog Proportional–Integral–Differential (PID) control system, which drives the fast piezoelectric actuator. Constant force is applied to a polyprotein chain by adjusting the position of the surface through the movement of the piezoelectric actuator. The PID insures a constant tension on the protein by monitoring the deflection of the cantilever.

In order to obtain several recoil traces from each stretched poly-protein we created a multi-quench protocol consisting in a fast ramp of force from –100 pN to 180 pN in 20 ms to maximize pick-up rate, followed by 0.2 s of constant force to allow all modules to unfold and finishing with a square wave force pattern lasting up to 1 s. The periodic stretching and quenching protocol is designed to keep the protein in its purely elastic regime, avoiding any enthalpic interactions that occur upon quenching the force to a much lower final value. Contrary to the unfolding events that are stochastic in nature, in this multi-quench protocol the stretching and recoil times are known in advance. We take advantage of this knowledge to optimize the control response by driving the actuator closer to the new equilibrium position by a distance equal to $k/\Delta F$ where k is the cantilever spring constant and ΔF is the magnitude of the stepwise change in force. This pre-emptive system leaves the PID control with a smaller task of driving only the change in length of the protein.

The cantilevers were calibrated using the equipartition theorem, and the contact slope was obtained by moving of the piezo-

cantilever ensemble. The physical properties of the cantilever used influence the response time and force sensitivity. The spring constant influences the signal to noise ratio of the measurement, while the resonance frequency limits the measurement bandwidth. Furthermore, the surface area of the cantilever perpendicular to the direction of motion induces opposing viscous drag forces. We analyzed three types of cantilevers fitted for the purpose of the experiment: Bruker MLCT (spring constant approximately 20 pN/nm, resonance frequency in water approximately 1 kHz), Olympus Biolever BL-RC150VB (spring constant approximately 40 pN/nm, resonance frequency approximately 9 kHz) and Olympus Biolever BL-AC40TS (spring constant approximately 100 pN/nm, resonance frequency approximately 25 kHz). Fig. S1 shows the drag response of three types of cantilevers as a function of moving velocity close to a surface. In this experiment the force experienced by cantilevers at different approach and redraw velocities was measured. As shown in Fig. S1A, the effect of the drag is symmetric around the zero force position (part 2 and 4 vs. part 1 of the trace). In part 3 the cantilever is in contact with the surface. The piezo's position protocol shown in lower box of Fig. S1A was applied to measure the deflection force curves (upper box of Fig. S1A and C), which were used to evaluate the drag coefficients. Fig. S1D shows the way in which the different cantilevers respond to the drag forces with respect to the velocity of the actuator. For our experiments we chose the Olympus Biolever BL-RC150VB, which exhibits good balance between the drag force and the force signal resolution.

In a typical experiment, the cantilever is pushed to the surface with a force of approximately 1 nN for 1 s, it is then retraced to a deflection corresponding to a force of 180 pN. At this force ubiquitin domains unfold and the end-to-end extension increases in steps of 20 nm, corresponding to the elastic extension of the amino acids trapped behind the mechanical transition state corresponding to the unfolding of the protein. Once unfolded, the polypeptide chain is cycled between 250 and 100 pN. After the polyprotein detaches the PID cannot maintain the set-point force anymore and drives the surface away from the cantilever at high velocity.

The final part of the curve, when the protein detaches and the surface is moved away from the cantilever at a PID specific velocity constitutes a second way to measure the drag. Fig. S2 shows such an experiment, where after detaching the cantilever experiences two force regimes. Each regime is characterized by a certain constant force and constant velocity. The drag coefficient is calculated then as the slope of the line fitted to the force and velocity of each stage, plotted one against the other (Fig. S2). The averaged values from all the gathered fits is 2.286 ± 0.481 pN·ms/nm, which agrees with the drag force measured independently from the cantilever itself.

The use of fast piezoelectric actuators and small cantilevers greatly improves the response time of the feed-back loop. Fig. S3 shows that the time needed to restore the constant force after an unfolding event is typically under 150 μs, while using just the PicoCube actuator and the slower MLCT cantilevers yields a response time of 4 ms.

High Force Approximation. The extension required to stretch an unfolded protein under constant force is typically approximated as resulting mainly from the entropy of the chain. The extension's dependency on the force is described by the worm-like-chain (WLC) model of elastic extension (2–4):

$$F(x) = \frac{k_B T}{p} \left[\frac{1}{4} \left(1 - \frac{x}{L_c} \right)^{-2} - \frac{1}{4} + \frac{x}{L_c} \right], \quad [\text{S1}]$$

where k_B is Boltzmann's constant, T is the absolute temperature, p is the persistence length, L_c is the contour length, and x denotes the end to end extension of the chain, which is also our reaction coordinate. We use a high force approximation to simplify the inversion of Eq. S1. According to this approximation, the linear term on the right hand side of Eq. S1 was taken to be $x/L_c = 0.5$. In this regime, where the force is high, the contribution of the linear term in Eq. S1 is less than 2%, and the function hardly changes with the extension when looking at the asymptote towards the contour length (Fig. S4).

$$x(F) = L_c \left[1 - \left(\frac{4pF}{k_B T} - 1 \right)^{-1/2} \right]. \quad [\text{S2}]$$

From the figure it is apparent that at the intercept between the two curves, at $x/L_c = 0.5$ $F \sim 13$ pN, above which the two curves are very close to each other, until $F \sim 50$ pN, where they coincide, making this approximation reasonable to use as long as we stay above these values.

Force Balance to Determine D_{eff} (Brownian Dynamics). D_{eff} determines the dynamics and time scales measured along the collapse and extension traces. With the application of an external constant force, F_i , the relaxation process is given by the following force balance (under the assumption of high force made above) along the reaction coordinate x , the end-to-end length:

$$\mu \frac{dx}{dt} + F_E(x) - F_i = 0, \quad [\text{S3}]$$

where μ is the damping coefficient, which is related to the diffusion coefficient, D_{eff} , by the Einstein relation $\mu = k_B T / D_{\text{eff}}$. $F_E(x)$ is the elastic force predicted by the WLC polymer elasticity model given by Eq. S2. Thus, Eq. S3 can be fully written:

$$\frac{dx}{dt} = -\frac{D_{\text{eff}}}{4p} \left(1 - \frac{x}{L_c} \right)^{-2} - \frac{D_{\text{eff}}}{4p} + \frac{D_{\text{eff}}}{k_B T} F_i \quad [\text{S4}]$$

which solves to give:

$$\frac{x}{L_c} = -\left| -\frac{x}{L_c} + \left(1 - \frac{1}{q} \right) \right| e^{\kappa e^{\alpha(1-\frac{x}{L_c})}} e^{\lambda(t-t_0)} + \frac{1}{q} + 1, \quad [\text{S5}]$$

where $q = \left(\frac{4pF_i}{k_B T} - 1 \right)^{1/2}$, $\kappa = \frac{D_{\text{eff}}}{2pL_c} \left(\frac{4pF_i}{k_B T} - 1 \right)^{3/2} C$, $\alpha = 2q$ and $\lambda = \frac{D_{\text{eff}}}{2pL_c} \left(\frac{4pF_i}{k_B T} - 1 \right)^{3/2}$ with C being an integration constant. Defining $y = -\frac{x}{L_c} + \left(1 - \frac{1}{q} \right)$, Eq. S5 turns into

$$y = |y| e^{\left(\frac{\kappa + \alpha}{q} \right) e^{\alpha y}} e^{\lambda(t-t_0)} - \frac{2}{q}. \quad [\text{S6}]$$

Taking $y > 0$ returns a false expression: $x < -L_c(1 - 1/q)$ because x , q , and L_c are positive numbers bigger than 1, hence y has to be taken as < 0 to give:

$$y e^{\alpha y} = -\frac{2}{q} e^{-(\kappa+2)} e^{-\lambda(t-t_0)}. \quad [\text{S7}]$$

Interestingly, this expression has both linear and exponential dependencies on x and t , a predicament which is best treated by the Lambert W function. This function is defined as the inverse

of $f(x) = x e^x$, which basically means that $x = W[f(x)]$ (5). In order to be formalized with the W function, Eq. S7 has to be rearranged:

$$y = \frac{1}{\alpha} W \left[-\frac{2}{q} e^{-(\kappa+2)} e^{-\lambda(t-t_0)} \right] \quad [\text{S8}]$$

and then solved:

$$x = x_0 - A W[-B e^{-\lambda(t-t_0)}] \quad [\text{S9}]$$

here $x_0 = L_c(1 - 1/q)$ corresponds to the plateau after the relaxation, $A = L_c/\alpha$, $B = (2/q) \exp[-(\kappa + 2)]$ and

$$\lambda \cong \frac{D_{\text{eff}}}{2pL_c} \left(\frac{4pF_i}{k_B T} \right)^{3/2} \quad [\text{S10}]$$

leading to the final expression:

$$x(t) = x_0 - A W \left\{ -B \exp \left[-\frac{D_{\text{eff}}}{2pL_c} \left(\frac{4pF_i}{k_B T} \right)^{3/2} (t - t_0) \right] \right\}. \quad [\text{S11}]$$

This expression was used to fit the traces to get D_{eff} . The simulations were performed in Igor Pro 6 platform (Wavemetrics). The simulated traces were generated by solving Eq. 1 in the main text with a time resolution of $5 \cdot 10^{-8}$ s. Fig. S5 below shows a fitting with Eq. S11 to a simulated trace (dashed black line) together with a single exponential, $x(t) = x_0 + A \exp(-t/\tau)$ (scattered red line) with their residuals. The single exponential was used to evaluate the relaxations time constants (Fig. 2 in the *main text*). Interestingly, Eq. S11 fits better the chain's relaxation than the exponential decay.

The fitted averaged D_{eff} value of 1,226 nm²/s used in the Brownian dynamics simulations remarkably returned a fitted averaged D_{eff} value of $1,214 \pm 39.81$ nm²/s for the collapse and $1,223 \pm 29.40$ nm²/s for the extensions. Interestingly, there is a variation in the spread of the experimentally observed D_{eff} 's fitted values when compared with the simulation's narrow distributions (Fig. 2C in the *main text* and Fig. S6). One of the most probable causes for this spread is the persistence length, p , used in the fits, which was assumed to have a constant value of 0.4 nm [a typical value for unfolded proteins (6, 7)]. However, it is evident that p can vary between 0.25 and 2.5 nm (8–11). Unlike the simulated traces, the measured traces shows a length diversity which was demonstrated to be determined to large extent by the strength of the entropic, hydrophobic and electrostatic interactions (8). These interactions result from considerable alterations in the chain's dihedral-space conformation together with side-chain packing of the collapsing structures. All these interactions are giving raise to length deviations from the WLC predictions and resulting with different persistence lengths. Nevertheless, we assumed here a constant value for p to keep the calculation simple and consistent.

Mechanical Impedance (Kelvin-Voigt Model). Frequency response function in physical systems is conveniently described by the Kelvin-Voigt circuit, which describe a simple mechanical structure consisting of a mass, a spring, and a dashpot. A force, $F(t)$, along one direction is applied and the system responds by changing the end-to-end length displacement, $x(t)$, accordingly. Here, we consider the over-damped scenario by neglecting the inertia term, thus describing the dynamic response of the system (the polypeptide) by its elasticity, k_{pol} and viscous damping coefficient, μ through its equation of motion:

$$F(t) = k_{\text{pol}} x(t) + \mu \dot{x}(t). \quad [\text{S12}]$$

The Kelvin-Voigt model assumes a linear constant parameter system. Therefore its dynamic can be described by a frequency response function, which is the Laplace transform of the system's output: $x(t) \Rightarrow x(\omega)$, where ω is the angular frequency, resulting in:

$$x(\omega) = \frac{F(\omega)k_{\text{pol}}}{k_{\text{pol}}^2 + \mu^2\omega^2} - i \frac{F(\omega)\mu\omega}{k_{\text{pol}}^2 + \mu^2\omega^2} = \text{Re}(\omega) - i\text{Im}(\omega). \quad [\text{S13}]$$

Here $\text{Re}(\omega)$ and $\text{Im}(\omega)$ denote the real and imaginary parts of the dynamic response. The output of the system in dB is given by

$$\text{dB} = -10 \log \left(\frac{\text{Amp}^2(\omega)}{\text{Amp}^2(0)} \right). \quad [\text{S14}]$$

Where $\text{Amp}^2(\omega)$ is the amplitude, given by $\text{Amp}^2(\omega) = \text{Re}^2(\omega) + \text{Im}^2(\omega)$ to give

$$\begin{aligned} \text{dB} &= 10 \log \left(\frac{1}{1 + (\mu\omega/k_{\text{pol}})^2} \right) \\ &= 10 \log \left(\frac{1}{1 + (2\pi f k_B T / k_{\text{pol}} D)^2} \right), \end{aligned} \quad [\text{S15}]$$

where $\omega = 2\pi f$, f being the frequency in Hz. The bandwidth frequency, $f_{1/2}$, serves as an important parameter for characterizing the frequency at which the mechanical response drops to half of its amplitude. $f_{1/2}$ is defined at -3 dB by

$$-3 = 10 \log \left(\frac{1}{1 + (2\pi f_{1/2} k_B T / k_{\text{pol}} D)^2} \right) \quad [\text{S16}]$$

$$f_{1/2} \approx \frac{k_{\text{pol}} D}{2\pi k_B T}. \quad [\text{S17}]$$

Using the WLC assumptions with a frictional term, Khatri, et al. introduced an expression for a polypeptide chain elasticity (12):

$$k_{\text{WLC}} = \frac{4}{L_c} \sqrt{\frac{p}{k_B T}} F^{3/2} \quad [\text{S18}]$$

when substituted into Eq. S17, we get the final expression for the bandwidth frequency dependency on the system's parameters:

$$f_{1/2} = \frac{2D\sqrt{p}}{\pi L_c} \left(\frac{F}{k_B T} \right)^{3/2}. \quad [\text{S19}]$$

Molecular Dynamics Simulations. All-atom simulations in explicit solvent were carried out with the software NAMD 2.8, using the CHARMM22 force-field with CMAP corrections for the protein, and the TIP3P water model. We used periodic boundaries conditions and a cutoff of 12 Å for electrostatic and Lennard-Jones interactions. Long-range electrostatic interactions were calculated using the PME method with a grid spacing of 1 Å. All bonds between light and heavy atoms were maintained rigid, while the rest of the protein was flexible. Steered MD simulations of wild-type ubiquitin (PDB ID code 1UBQ) were performed by fixing the C α of the first residue (MET1) and by applying a constant force on the C α of the last residue (GLY 76) along the z direction.

System preparation: To unfold the protein, we first pull on ubiquitin molecule in vacuum at a high force of 800 pN, during 10 ns. A fully extended protein was thus generated, with no remaining secondary structure. It was then solvated using the waterbox module of VMD in a box of 3.5 * 3.5 * 32 nm, comprising 11,499 water molecules and 35,728 atoms total. Energy minimization using the steepest descent method (2,000 steps) was performed before further equilibration, as described below.

Equilibration: The protein was then equilibrated for 6 ns at 250 pN in the isobaric ensemble at 300 K and 1 bar, using a time-step of 2 fs, a Langevin thermostat (damping coefficient of 1 ps⁻¹) for temperature control and the modified NAMD version of the Nose-Hoover barostat with Langevin dynamics (piston period of 0.1 ps and piston decay time of 0.05 ps) for pressure control. This simulation was then propagated for 25 more ns to check that the average end-to-end distance no longer evolved. No dynamical data was extracted from these simulations because of possible bias introduced by the temperature and pressure control.

Collapse simulations: Initial configurations for collapse from 250 pN to 100 pN were chosen along the 25-ns trajectory at 250 pN. The simulations were propagated in the micro-canonical ensemble for 5 ns to avoid spurious effects from pressure and temperature control on the dynamics of collapse. A time-step of 1 fs was used. We performed five such simulations to obtain the average relaxation. Because of the large system size, average temperature and pressure along these trajectories are very close to that targeted during the NPT equilibration.

Extension simulations: The last configuration of one of the collapse trajectory was then propagated for 30 ns using the same setup as for equilibration (NPT ensemble), both to check convergence of the end-to-end distance and to generate starting configurations for extension: finally, five such trajectories were generated by pulling back the protein at 250 pN during 5 ns in the NVE ensemble.

Diffusion coefficient: To estimate the diffusion coefficient along the end-to-end coordinate, we have employed a method described earlier (13, 14). At each given force an additional 3-ns simulation in the micro-canonical ensemble is performed using the collective-variable module of NAMD to add a bias potential on the end-to-end distance. This potential is harmonic and chosen to be much stiffer than the actual PMF on which the protein is moving, so that the resulting PMF is locally harmonic. Under this approximation, it can be shown that the diffusion coefficient can be recovered from the time autocorrelation function of the end-to-end distance L ,

$$D = \frac{\langle \delta L^2 \rangle^2}{\int_0^\infty \langle \delta L(t) \delta L(0) \rangle dt}, \quad [\text{S20}]$$

where $\delta L = L - \langle L \rangle$ are the fluctuation of L around its average value. We performed simulations at both forces (100 pN and 250 pN), using a force constant of 100 kcal/mol/Å² to constraint the system around the average end-to-end distance $\langle L \rangle$ estimated from unperturbed simulations (25.5 nm at 250 pN and 23.7 nm at 100 pN). In both cases, the unperturbed PMF is very smooth in this region and we checked on a smaller, model system (decaalanine in water) using different values for the force constant (20, 50, and 100 kcal/mol/Å²) that it does not have any significant impact on the obtain value of D .

An example of the average autocorrelation function of L is shown in Fig. S7. Error bars on D are estimated from block averaging and by estimating D independently for each block. A manuscript presenting further details about this approach and other new insights from MD simulations is currently in preparation.

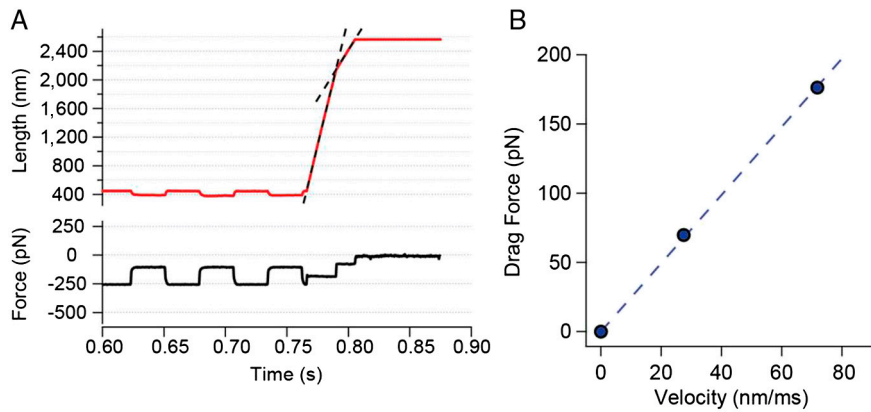


Fig. S2. Drag force measurements from constant force AFM experiments. (A) An experiment example, in which an unfolded poly-ubiquitin chain is stretched and relaxed between 250 and 100 pN. The piezo actuator is rapidly moved away from the cantilever as the chain ruptures at approximately 0.77 s. (B) Force vs. velocity of the two stages detected after the detachment, out of which the drag coefficient is estimated per molecule from the slope of the linear fit between the points.

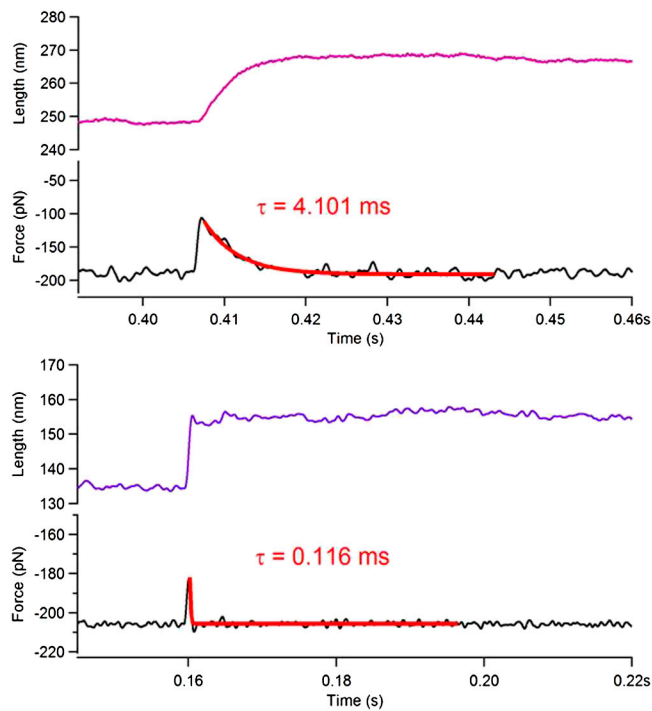


Fig. S3. Two force traces of a single ubiquitin unfolding. The control system responds to the unfolding event driving the actuator withdraw the protein and recover the condition of constant force. Force trace obtained by a standard AFM that shows decay with a time resolution of 4 ms (upper box). The new fast-AFM used in this work shows an almost instantaneous force recovery with a time constant smaller than 150 μ s under the same conditions (low box).

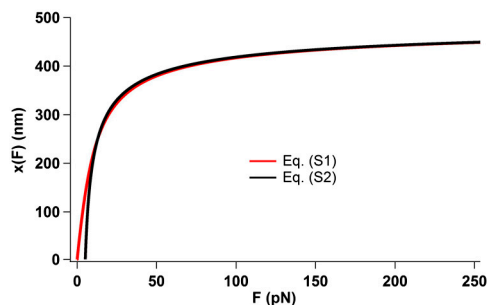


Fig. S4. Comparison between the phenomenological WLC model, given by Eq. S1 (red) and its high force modification, Eq. S2 (black). From forces above 50 pN the two curves coincide.

